Original Research Article

Synthesis spectral charecterization of chalcone: Structural elucidation through single-crystal XRD, Hirshfeld surface analysis,and DFT calculations

ABSTRACT

Organic compound (E)-6-(3-(p-tolyl)acryloyl)-2H-benzo[b][1,4]oxazin-3(4H)-one [6TABO] with molecular formula $C_{18}H_{15}NO_3$ was synthesized using Claisen–Schmidt condensation reaction method. FT-IR and ^1H NMR spectra were recorded to identify the various functional groups present in the compound and confirm the chemical structure.The UV–Visible spectrum study reveals that the crystal is transparent in the entire visible region and the absorption is observed at 325.40 nm. Single-crystal XRD studies show that the compound crystallizes in the monoclinic system with a space group P 1 21/c 1. The corresponding lattice parameters of the crystal are a = 13.0723 (7) Å, b = 7.1789 (4) Å, c = 16.1812 (9) Å, $\alpha=90^0$, β = 109.148 (2)^0, $\gamma = 90^0$.The Hirshfeld surface and 2-D fingerprint analysis were performed to study the nature of interactions and their quantitative contributions towards the crystal packing. Structure determination was optimized by Density Functional Theory (DFT) using B3LYP/6-311G++(d, p) method in the ground state.

Keywords: Chalcones, Single crystals, Hirshfeld surface,Fingerprint plots,DFT studies.

INTRODUCTION

Chalcone compounds are-unsaturated ketone involving the reactive keto-ethylenic group (CO-CH=CH-) which gave colored compounds due to the presence of (CO-CH=CH) the chromophore group [1-5].Molecular Hirshfeld surface [6, 7] analysis in the crystal depicts a method to study the nature of the intermolecular interactions using a partitioning of crystal space in an innovative visual manner. The associated fingerprint plots [8] represent the intermolecular interaction in a convenient color plot.

Experimental section

Instruments

The IR spectrum was recorded in AVATAR-330 FT-IR spectrophotometer and only noteworthy absorption levels (reciprocal centimeters) were listed. ^{1}H NMR spectra were recorded at 300 and 400 MHz on Bruker AMX 300 and 400 MHz spectrophotometers using CDCl3 as solvent and TMS as internal standard. The reactions and the purity of the products were assessed by performing TLC. All the reported melting points were taken in open capillaries andwere uncorrected.

Synthesis

The ethanolic solution of 6-Acetyl-2H-1,4-benzoxazin-(4H)-3one (0.4716g) andp-methylbenzaldehyde (0.7642g) was stirred with a small quantity of N/10 sodium hydroxide solution for 4 hours. The resulting solution was poured into ice-water and the formed precipitate was filtered. The crude Chalcone was recrystallized from ethanol.

Reaction

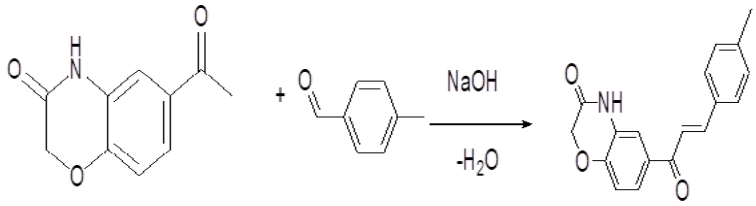

Table 1

Compound	Molecular formula	Molecular weight	Melting point(^{0}C)
6TABO	$C_{18}H_{17}NO_3$	295.3	148.9

RESULTS AND DISCUSSION

ANALYSIS OF FT-IR SPECTRUM

Infrared Spectroscopy gives information on molecular vibration or more precisely on transitions between vibrational and rotational energy levels in molecules.

Absorption of radiation in the infrared region results in the excitation of bond deformations, either stretching or bending, various stretching and bending vibrations occur at certain quantized frequencies. When infrared light of that frequency is incident on the molecule, energy is absorbed and the amplitude of that vibration is increased. The infrared spectrum is obtained when the frequency of molecular vibration corresponds to the frequency of the infrared radiation absorbed. The vibrational frequency depends on the force constant and reduced mass of the atom. The influence of small changes in molecular structure on vibrational frequencies is a mesomeric effect, inductive effect, field-effect, steric effect and hydrogen bonding, etc. The carbonyl group in conjugation with the double bond /aromatic ring results in the delocalization of the π electrons of both unsaturated groups and reduces the double bond character of carbonyl frequency. The lowering of absorption frequencies of both >C=C< and>C=O groups are attributed to the resonance as shown below:

The introduction of the double bond in conjugation with carbonyl group also lowers the vibrational frequency to 1646 cm^{-1} and C=C stretching frequency observed at 1610 cm^{-1}. The presence of absorption bands at 1560, 1509, and 1485 $cm^{-1}$is due to the aromatic skeletal stretching.

The structure frequency at 3234 cm^{-1} is due to the oxazinyl >N-H. The amide >C=O group of benzooxazinyl moiety appears at 1686 cm^{-1}**(Fig-1).**

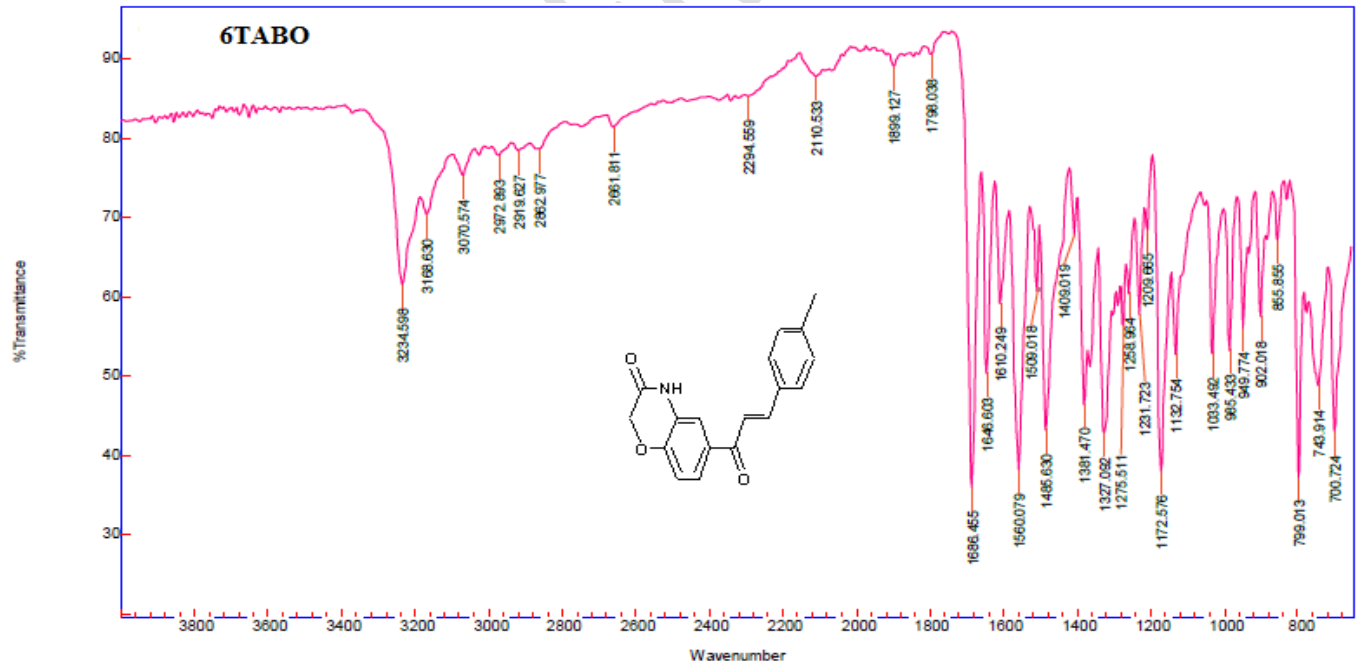

Fig-1. FT-IR Spectrum of compound 6TABO

^{1}H NMR SPECTRA

There has been considerable interest in the literature in recent days to correlate chemical shifts if proton with substituent constants in various system. Dhami and Stothers[9,10] have extensively studied the ^{1}H NMR spectrum of a large number of acetophenones and styrenes with a view to establish the validity of the additivity of substituent effects on aromatic shildings., Leterbur[11]measured the ^{1}H NMR spectrum of α,β-unsaturated carbonyl compounds of the type RC6H4-CH=CH-CO-CMe_3 and sought Hammett correlations for the ethylenic protons. In general, the signals for aromatic protons present in a molecule appear in the downfield region of around 7 ppm due to magnetic anisotrophic effect. In most of the cases, since the absorption of the olefinic protons in the chalconesare also in the aromatic region, it is quite difficult to differentiate the olefinic proton signals from that of the aryl protons.

Generally of the two olefinic protons in chalcones, the one nearest to the aromatic ring (H_β proton) resonates in the deshielding region compared to that of α-proton (H_β) because this will experience a magnetic field from the induced circulation of π electrons in the aromatic ring, which will augment the applied field and hence lead to a higher δ value.

The signals of the ethylenic proton in the compound investigated in the study are assigned. The ethylenic proton (Hα and Hβ) signal appears as doublet and are well separatedfrom the signals of the aromatic protons.

H_β proton shift for the compound 6TABO lies in 7.753 ppm and the Hα proton resonates at 6.988 ppm.

The peak at 4.654 ppm is due to the protons of oxazinyl methane group.

The singlet at 8.082 ppm is to assigned the >NH proton. The singlet in the up field region (2.332 ppm) is due to methyl protons in the p-position of the phenyl ring.**(Fig-2).**

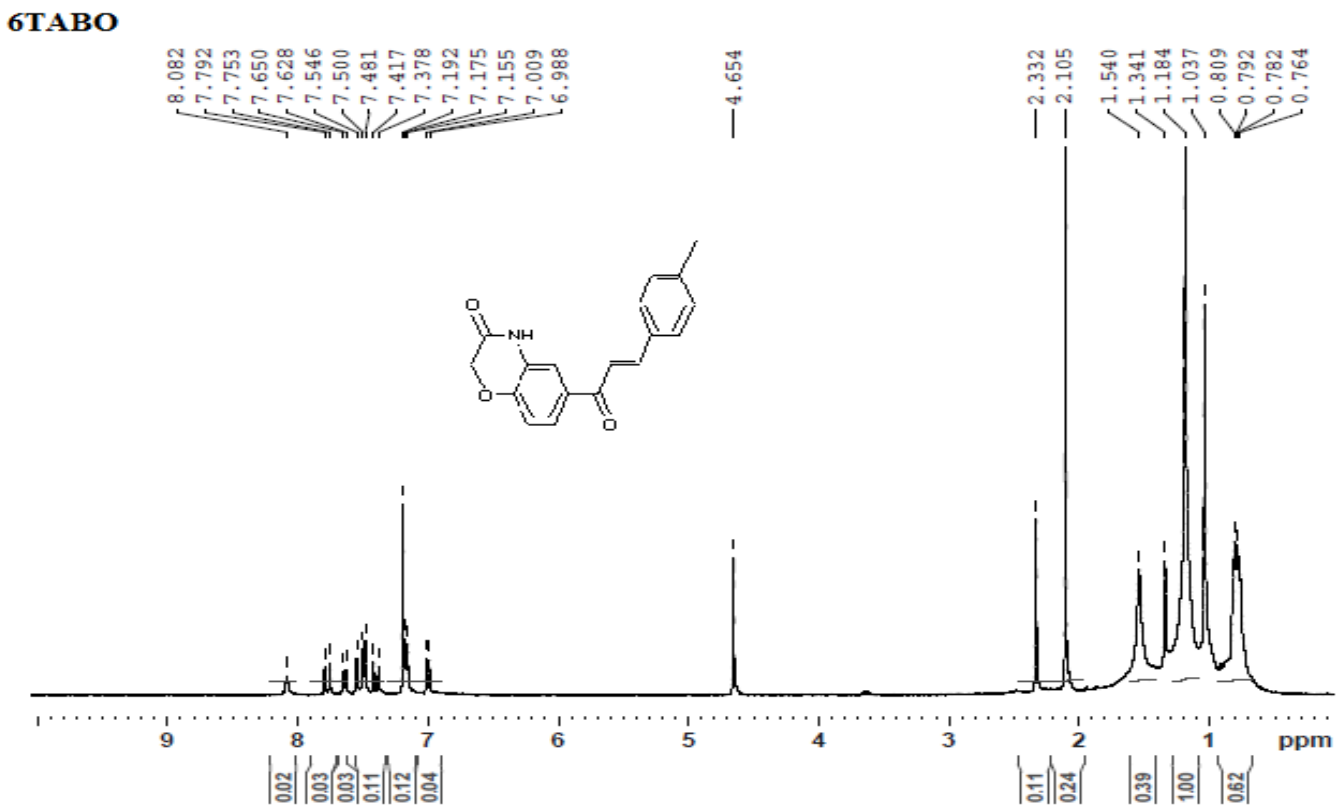

Fig-2.^{1}H NMR Spectrum of compound 6TABO

UV ABSORPTION SPECTRUM

The recorded UV spectrum for the new compound is shown in Fig. 3. Most of the absorption spectroscopy of organic compounds is based on transitions of n or π electrons to the π* excited state which takes place in the range 200–700 nm. In this point of view, the max absorption peak observed at 325.40 nm (Fig. 3) can be assigned to n → π* transition and may be attributed to the excitation in the aromatic ring and C=O group [29].

Table 2
UV spectral data of compound 6TABO

Solvent	λ_{max}	γ_{abs} cm^{-1}
CCl_4	325.40	1.196

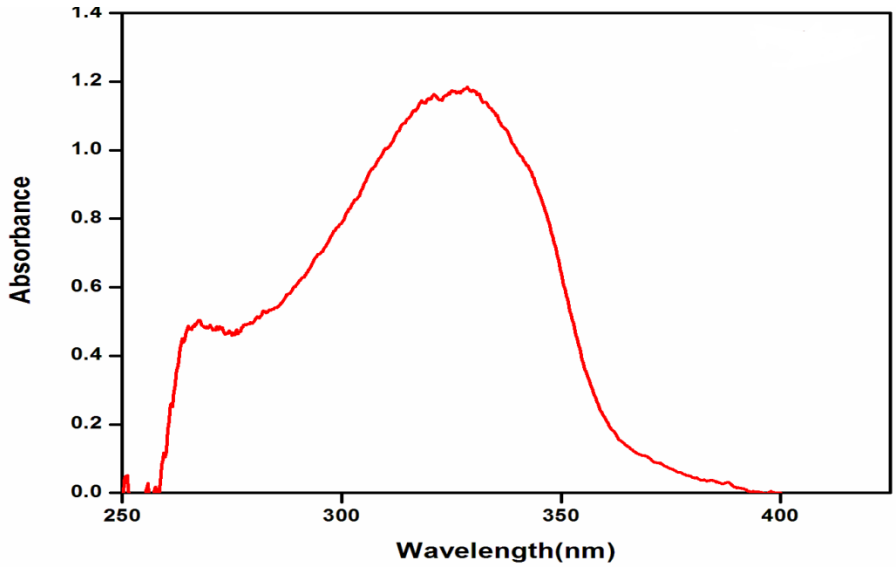

Fig-3.The UV absorption spectrum of compound 6TABO in CCl_4

X-ray crystallographic analysis of compound 6TABO

The compound (**6TABO**) is characterized by spectral studies and single-crystal X-ray analysis. The compound crystallizes in the monoclinic space group P 1 21/c 1 with the following unit cell parameters: a = 13.0723 (7) Å, b = 7.1789 (4) Å, c = 16.1812 (9) Å, $\alpha=90^0$, $\beta = 109.148\ (2)^0$, $\gamma = 90^0$. The crystal structure was solved by direct methods using single-crystal X-ray diffraction data collected at 302 (2) K and refined by full-matrix least-squares procedures to a final R-value of 0.0645 for 0.1794 observed reflections. The crystal ORTEP structure and packing diagram Figs. **4** and **5**. Crystal data and details of the structure determination of the compound **6TABO**shows in **Table-3**, selected bond lengths (Å), bond angles (^{0}), Torsion angles (^{0}), of the compound **39** are shown in Table **4-6**.

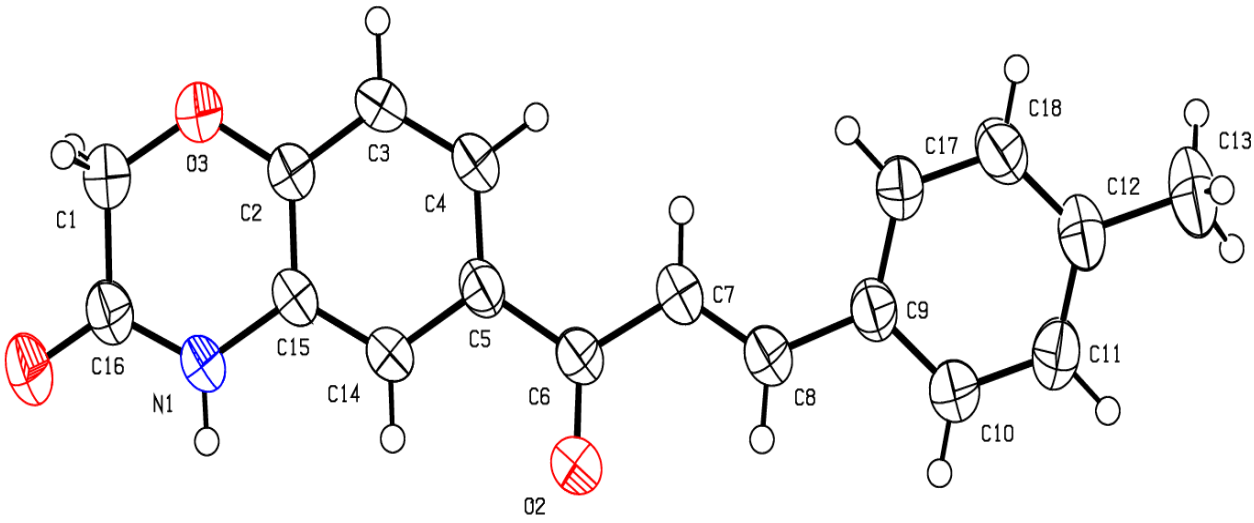

Fig-4. ORTEP structure of compound 6TABO

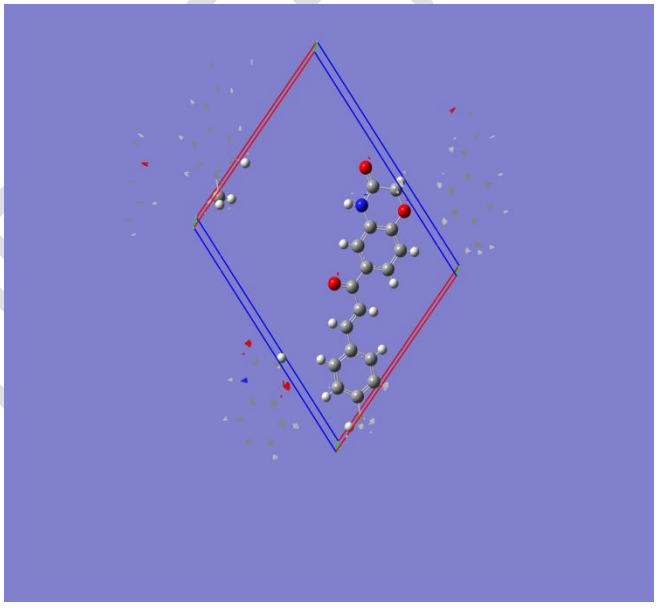

Fig-5. Packing diagram of compound 6TABO

Table-3: Crystal data and details of the structure determination of the compound 6TABO

Empirical Formula	$C_{18}H_{15}NO_3$
Formula weight	293.31 g/mol
Crystal system	monoclinic
Space group	P 1 21/c 1
Cell constant	-
a (Å)	13.0723(7)
b (Å)	7.1789(4)
C (Å)	16.1812(9)
α (Å)	90°
β (Å)	109.148(2)°
γ (Å)	90°
Volume ($Å^3$)	1434.51(14)
z	4
Crystal size (mm)	0.210x 0.290x 0.350
Radiation	**Mo Ka** λ =0.71073Å
Temperature Θ limits (°) Index range	302(2) K 2.67 to 30.11° -18<= h <= 18, -10<= k <= 10, -22<= 1 <= 22,
Reflections collected	21206
Goodness-of-fit	1.222
Completeness	99.2%

Table-4: Selected bond lengths (Å) of the compound 6TABO

Bond Lengths			
O1-C16	1.223(2)	02-C6	1.233(2)
03-C2	1.362(2)	O3-C1	1.390(2)
N1-C16	1.334(2)	N1-C15	1.4005(19)
N1-H1A	0.86	C1-C16	1.501(3)
C1-H3	0.97	C1-H1	0.97
C2-C3	1.376(2)	C2-C15	1.385(2)
C3-C4	1.382(3)	C3-H4	0.93
C4-C5	1.387(3)	C4-H5	0.93
C5-C14	1.398(2)	C5-C6	1.475(2)
C6-C7	1.467(2)	C7-C8	1.328(3)
C7-H7	0.93	C8-C9	1.458(2)
C8-H8	0.93	C9-C10	1.384(3)
C9-C17	1.389(3)	C10-C11	1`374(2)
C10-H11	0.93	C11-C12	1.381(3)
C11-H10	0.93	C12-C18	1.38493
C12-C13	1.504(2)	C13-H12	0.96
C13-H2	0.96	C13-H13	0.96
C14-C15	1.37892)	C14-H6	0.93
C17-C18	1.374(2)	C17-H14	0.93
C18-H9	0.93		

Table-5: Selected bond Angles (°) of the compound 6TABO

Bond Angles			
C2-O3-C1	120.12(15)	C16-N1-C15	123.35(16)
C16-N1-H1A	118.3	C15-N1-H1A	118.3
O3-C1-C16	119.58(16)	O3-C1-H3	107.4
C16-C1-H3	107.4	O3-C1-H1	107.4
C16-C1-H1	107.4	H3-C1-H1	107
O3-C2-C3	118.29(17)	O3-C2-C15	121.10(15)
C3-C2-C15	120.61(17)	C2-C3-C4	119.81(17)
C2-C3-H4	120.1	C4-C3-H4	120.1
C3-C4-C5	120.88(16)	C3-C4-H5	119.6
C5-C4-H5	119.6	C4-C5-C14	118.26(16)
C4-C5-C6	123.90(15)	C14-C5-C6	117.82(16)
O2-C6-C7	120.43916)	O2-C6-C5	119.11(15)
C7-C6-C5	120.46(16)	C8-C7-C6	121.13(18)
C8-C7-H7	119.4	C6-C7-H7	119.4
C7-C8-C9	128.62(19)	C7-C8-H8	115.7
C9-C8-H8	115.7	C10-C9-C17	116.96(17)
C10-C9-C8	119.10(17)	C17-C9-C8	123.94(18)
C11-C10-C9	121.97(18)	C17-C10-H11	119
C9-C10-H11	119	C10-C11-C12	120.98(19)
C10-C11-H10	119.5	C12-C11-H10	119.5
C11-C12-C18	117.30917)	C11-C12-C13	120.9(2)
C18-C12-C13	121.84(19)	C12-C13-H12	109.5
C12-C13-H2	109.5	H12-C13-H2	109.5
C12-C13-H13	109.5	H12-C13-H13	109.5
H2-C13-H13	109.5	C15-C14-C5	121.19(16)
C15-C14-H6	119.4	C5-C14-H6	119.4
C14-C15-C2	119.23(15)	C14-C15-N1	121.28(16)
C2-C15-N1	119.49(16)	O1-C16-N1	123.91(18)
O1-C16-C1	119.76(17)	N1-C16-C1	116.32(16)
C18-C17-C9	120.94(18)	O18-C17-H14	119.5
C9-C17-H14	119.5	C17-C18-C12	121.82(180
C17-C18-H9	119.1	C12-C18-H9	119.1

Table-6: Torsion angles (°) of the compound 6TABO

C2-O3-C1-C16	-0.6(3)	C1-O3-C2-C3	178.0(2)
C1-O3-C2-C15	-1.1(3)	O3-C2-C3-C4	179.60(18)
C15-C2-C3-C4	-1.3(3)	C2-C3-C4-C5	-0.3(3)
C3-C4-C5-C14	1.2(3)	C3-C4-C5-C6	-177.22(18)
C4-C5-C6-O2	167.02(19)	C14-C5-C6-O2	-11.4(3)
C4-C5-C6-C7	-12.9(3)	C14-C5-C6-C7	168.72(15)
O2-C6-C7-C8	6.8(3)	C5-C6-C7-C8	-173.29(16)
C6-C7-C8-C9	-179.58(16)	C7-C8-C9-C10	-170.64(19)
C7-C8-C9-C17	9.5(3)	C17-C9-C10-C11	0.7(3)
C8-C9-C10-C11	-179.12(18)	C9-C10-C11-C12	0.9(3)
C10-C11-C12-C18	-1.4(3)	C10-C11-C12-C13	178.52(18)
C4-C5-C14-C15	-0.6(3)	C6-C5-C14-C15	177.95(16)
C5-C14-C15-C2	-1.0(3)	C5-C14-C15-N1	178.83(15)
O3-C2-C15-C14	-179.00(17)	C3-C2-C15-C14	1.9(3)
O3-C2-C15-N1	1.2(3)	C3-C2-C15-N1	-177.92(17)
C16-N1-C15-C14	-179.22(17)	C16-N1-C15-C2	0.6(3)
C15-N1-C16-O1	178.83(16)	C15-N1-C16-C1	-2.1(3)
O3-C1-C16-O1	-178.8(2)	O3-C1-C16-N1	2.1(3)
C10-C9-C17-C18	-1.7(3)	C8-C9-C17-C18	178.10(17)
C9-C17-C18-C12	1.2(3)	C11-C12-C18-C17	0.4(3)
C13-C12-C18-C17	-179.55(18)		

Frontier molecular orbitals and molecular electrostatic potential

FMO analyses have been considered excellent in predicting the chemical stability of the molecules under investigation [12]. The lowest unoccupied molecular orbital (LUMO) and highest occupied molecular orbital (HOMO) is very important quantum orbitals. Usually, the LUMO expresses the capacity of accepting an electron while HOMO denotes the electron donation ability [13]. The HOMO-LUMO energy gap is an important parameter for predicting the chemical reactivity and dynamic stability of molecules [14].Furthermore, the prediction of the energy difference between FMOs is a wonderful sign for a lot of important variables such as

chemical hardness (η), global softness (S), and polarizability (α). It is well known that low energy gap of the FMO, as well as high polarizability,is better characteristics for good NLO compounds [15]. Fig. 6 illustrates the calculated energies difference and the ground state isodensity surface plots for the FMOs of 6TABO was shown in Table 7, the FMO energy gap and the global softness (S) were affecting by the length and the conformation of the alkoxy chain. As the length of terminal wings increase, the global softness and the polarizabilityincrease. Consequently, it is predicted that as the length of the alkoxy chains increases, their characteristics improve to be more proper candidates in nonlinear optical applications, Table 7.

Compound 6TABO				
Dipole Moment		**5.9703**		
HOMO	**LUMO**	**ΔE (E_{LUMO}-E_{HOMO})**	**η = ΔE(E_{LUMO}-E_{HOMO})/2**	**S = 1/ΔE = (1/2η)**
E_{HOMO} (a.u) -0.23701	**E_{LUMO} (a.u)** -0.09593	0.14108	0.07054	7.088177
E_{HOMO-1} (a.u) -0.24516	**E_{LUMO+1} (a.u)** -0.04890	0.19626	0.09813	5.095282
E_{HOMO-2} (a.u) -.026224	**E_{LUMO+2} (a.u)** -0.03780	0.22444	0.11222	4.455534
E_{HOMO-3} (a.u) -0.26304	**E_{LUMO+3} (a.u)** -0.3144	0.2316	0.1158	4.317789

Table-7.Molecular orbital energies, hardness (η), and global softness (S) of 6TABO

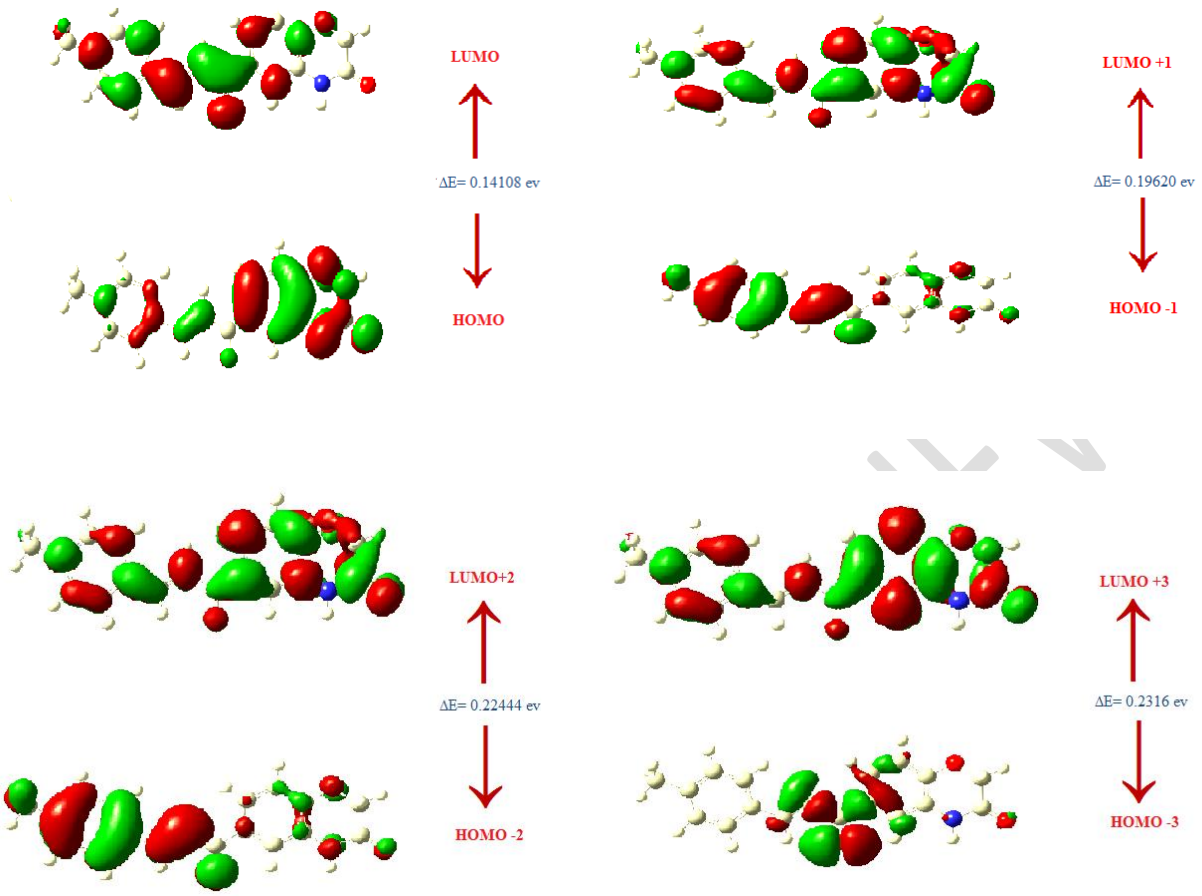

Fig. 6. The calculated ground state isodensity surface plots for frontier molecular orbitals of 6TABO

Mulliken charges distribution

The natural population analysis of the chalcone derivative is obtained by Mulliken. It describes the distribution of charges in the various sub-shells (core, valance, Rydberg) in the molecular orbital. The accumulation of natural charges on individual atom of the title molecule is given in the Table 8. Mulliken atomic charge calculation has an important role for the application of quantum chemical calculation of the molecular system. Atomic charge affects dipole moment, polarizability, electronic structure and other molecular properties of the system. Atoms represented by colours according to its Mulliken charges and graphical representation was shown in Fig.7

Atoms	Mulliken Charges	Atoms	Mulliken Charges	Atoms	Mulliken Charges
C_1	0.392829	H_{13}	0.220595	C_{25}	-0.090027
C_2	0.212872	C_{14}	0.508612	C_{26}	-0.152129
C_3	-0.192027	N_{15}	-0.794911	C_{27}	0.055655
C_4	-0.037183	H_{16}	0.355994	C_{28}	-0.155310
C_5	-0.130909	O_{17}	-0.384455	C_{29}	-0.166850
C_6	-0.114917	C_{18}	0.169208	H_{30}	0.155414
H_7	0.173574	C_{19}	-0.153641	H_{31}	0.152237
H_8	0.164291	H_{20}	0.196551	H_{32}	0.157437
H_9	0.200460	C_{21}	-0.173340	H_{33}	0.163726
O_{10}	-0.497500	H_{22}	0.183777	C_{34}	-0.612695
C_{11}	-0.255711	O_{23}	-0.393198	H_{35}	0.198738
H_{12}	0.234452	C_{24}	0.016589	H_{36}	0.189962
				H_{37}	0.201829

Table 8. Mulliken Atomic Charges at B3LYP/6-311++G(d,p)

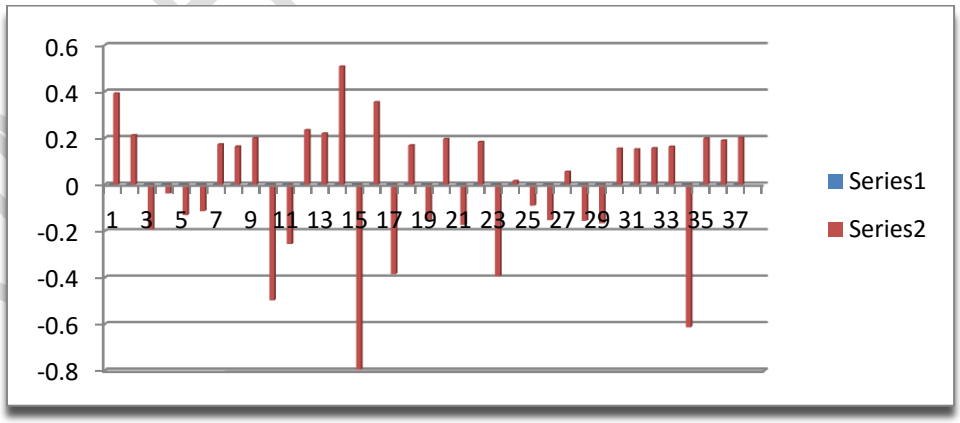

Fig.7.Mulliken Charges and graphical representation at B3LYP/6-311++G(d,p)

Molecular Electrostatic Potential (MEP)

The electrostatic potential that is made in the space around a particle by its cores and electrons (treated as static conveyances of charge) is an exceptionally valuable property for breaking down and foreseeing sub-atomic responsive conduct.

The potential has been especially valuable as a marker of the destinations or areas of a particle to which an drawing nearer electrophile and nucleophile is at first drawn in. The atomic electrostatic potential (MEP) is connected to the electronic thickness and is extremely helpful descriptor for deciding destinations for electrophilic assault and nucleophilic responses just as hydrogen-holding associations. The responsive locales for electrophilic and nucleophilic assault for HMHP-I, is displayed in Fig.8. With MEP investigation, the responsive destinations can be situated by various shading codes. The Red tone in the MEP realistic demonstrates an Electron-rich site which is a negative locale showing Electrophilic reactivity. The Blue tone in the MEP realistic shows an Electron-lacking site, which is a positive locale showing Nucleophilic reactivity. Furthermore, the Green tone in the MEP realistic shows the impartial, zero electrostatic potential locale showing Hydrogen-holding connections.

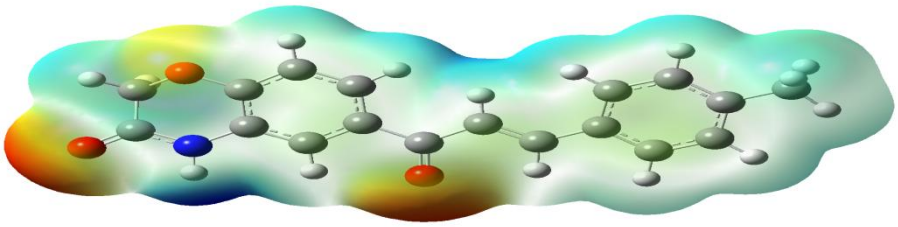

Fig.8. MEP Reactive Sites Calculated at B3LYP/6-311++G(d,p)

Hirshfeld surface analysis

The Hirshfeld surface has become a valuable tool for analyzing intermolecular interactions in a novel visual manner [16]. Hirshfeld surfaces of molecules are generated by partitioning space in the crystal into regions where the electron distribution of a sum of spherical atoms for the molecule (promolecule) dominates the corresponding sum over the crystal (procrystal). The Hirshfeld surface is the 0.5 isosurface for the normalized weighted electron density (or weight function w(r) = 0.5), a density that is defined as the ratio of the electron density for the promolecule to the electron density for the procrystal [17, 18].

$$w(r) = \frac{\sum_{a\varepsilon\, molecule}[\rho_a(r)]}{\sum_{a\varepsilon\, crystal}[\rho_a(r)]} = \frac{\rho_{promolecule}(r)}{\rho_{procrystal}(r)} \qquad \text{----------(1)}$$

Hirshfeld surfaces and their related fingerprint plots are generated using the program Crystal Explorer 3.0 [19]. The Crystallographic Information File (.cif) file of single-crystal X-ray diffraction is used as input to the Crystal Explorer program. The Hirshfeld surface is unique for a given crystal structure and a set of spherical atomic electron densities. For each point on that 3D Hirshfeld surface, two distances are specified: the distance from the Hirshfeld surface to the nearest nucleus inside the surface di and the distance from the surface to the nearest nucleus outside the surface de. Then dnorm is a normalized contact distance, which is defined in terms of di, de, and the van der Waals (vdW) radii of the atoms [20, 21].

$$d_{norm} = \frac{d_i - r_i^{vdw}}{r_i^{vdw}} + \frac{d_e - r_e^{vdw}}{r_e^{vdw}} \qquad \text{----------(2)}$$

The-Fig. 9 is obtained by mapping dnorm over the Hirshfeld surface. It also displays intermolecular interactions with the neighboring molecules. The surfaces are shown as transparent to allow visualization of the orientation and conformation of the functional groups inside the surface. The C–H···O hydrogen bonds are shown by green dotted lines. The dnorm values [22, 30, 31] are mapped over the Hirshfeld surface by using a red–white–blue color scheme where red regions represent closer contacts with a negative dnorm value, white regions represent the distance of contacts exactly comparable to the Van der Waals separation with a dnorm value of zero and blue regions represent longer contacts with a positive dnorm value. In dnorm surfaces, the large circular deep red colored depressions indicate hydrogen-bonding contacts and other spots are due to H–H contacts.

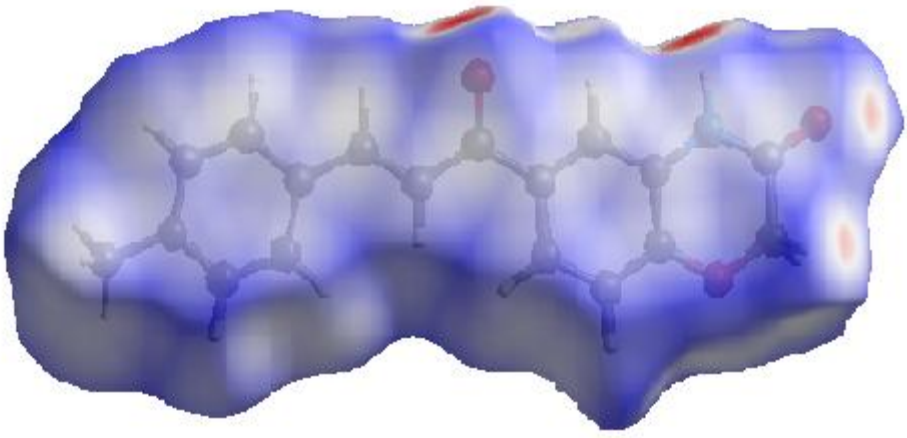

Fig.9- Hirshfeld surface of compound 6TABO

The 2-D fingerprint plots quantitatively give the nature and type of intermolecular contacts experienced by the molecules in the crystal. It plots the distance (di) from the nearest atom inside the surface against the distance (de) to the nearest atom external to the surface. The two-dimensional fingerprint plots are constructed by binning (di, de) pairs and coloring each bin as a function of the fraction of surface points in that bin, ranging from blue (few points) through green (moderate fraction) to red (many points). The outline of the full fingerprint is shown in grey color [23- 31].

In this analysis the different interactions can be separated from each other that would commonly overlap in full fingerprint plots. The 2-D fingerprint plots of the compound for all major intermolecular interactions with their percentage of contribution to the total Hirshfeld surface area for the molecule is shown in Fig. 10. The 2-D fingerprint plot for all the intermolecularinteractions are shown in Fig. 10a.The H···H interactions which are reflected in the middle of scattered points and cover most of the area in the 2-D fingerprint plots is shown in Fig. 10b, exhibit the most significant contribution of 47.31% to the total Hirshfeld surfaces. The H···O hydrogen bonding intermolecular interactionsin the 2D fingerprint plots, contributes 11.51% to the total Hirshfeld surfaces is shown in Fig. 10c.The C···C (Fig.10d.) and C···H interactions (Fig.10e.) in the 2D fingerprint plots contributes 14.2% and 5.8% to the total Hirshfeld surfaces. Hence both Hirshfeldsurfaces and fingerprint plots facilitate the comparison of intermolecular interactions in building supramolecular motifs in the crystal structure.

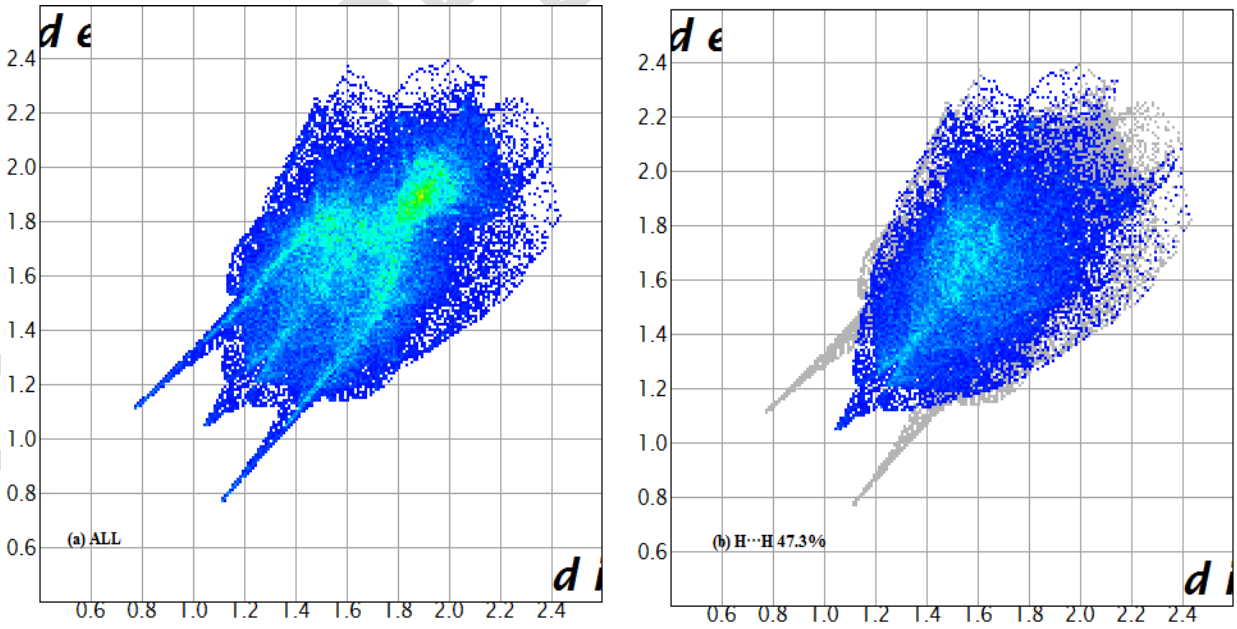

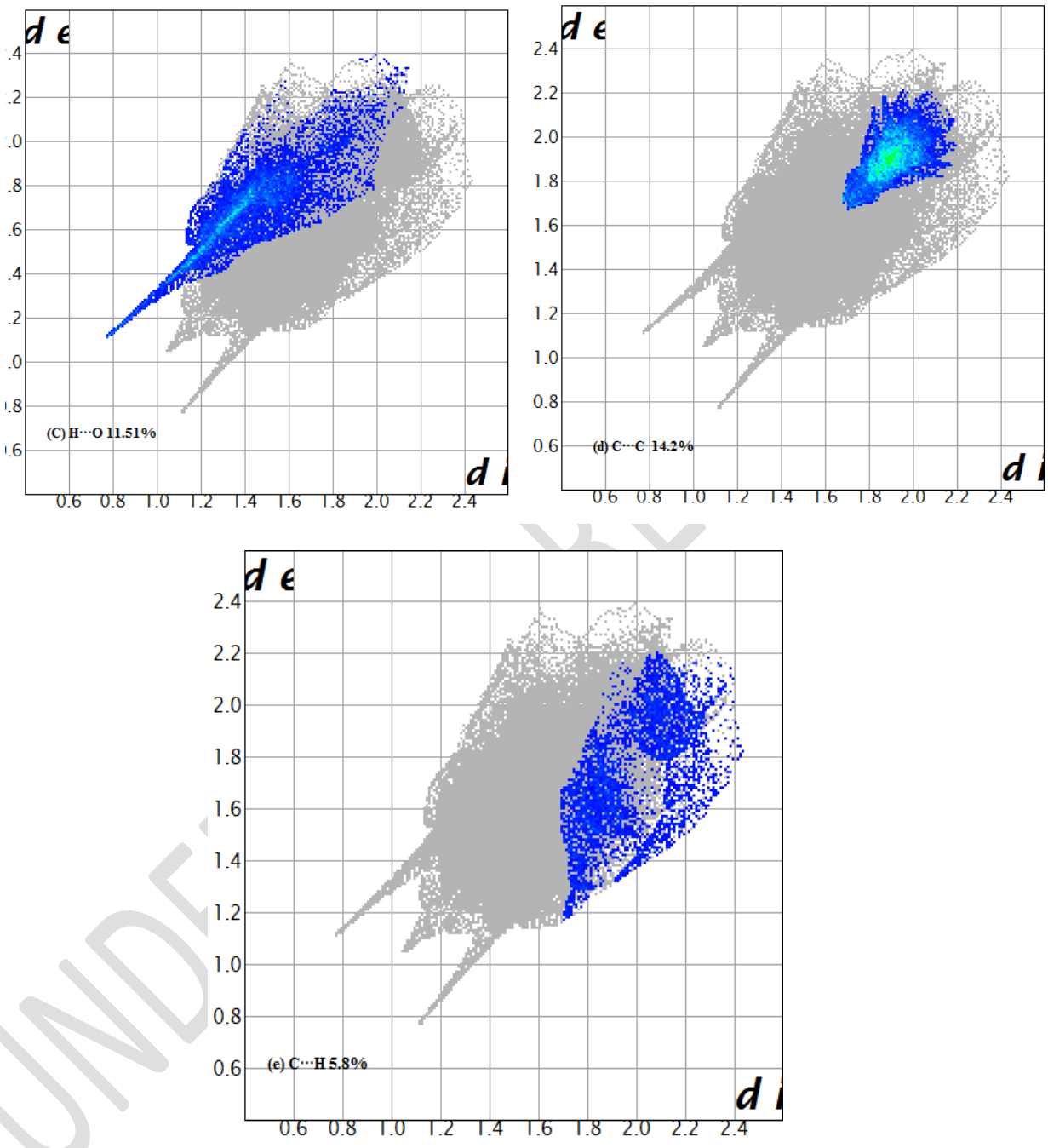

Fig. 10. Fingerprint plots of the compound where di and de are in Å

(a) The total contribution from all the interactions (b) H···H, (c) H···O, (d) C···C, (e) C···H, showing the percentage of contacts contributed to the total Hirshfeld surface area for the molecule. Blue color represents a low percentage of contacts and green a moderate percentage of contacts and outline of the full fingerprint is shown in grey.

Conclusion

A new chalcone derivative (E)-6-(3-(p-tolyl)acryloyl)-2H-benzo[b][1,4]oxazin-3(4H)-one [6TABO] has been synthesized using the Claisen–Schmidt condensation reaction method. The structure is confirmed with the help of FT-IR spectra and ^{1}H NMR spectrum.Crystal parameters are determined by single-crystal XRD study.The UV–visible study of MMPP indicates that the crystal is transparent in the entire visible range.

COMPETING INTERESTS DISCLAIMER:

Authors have declared that no competing interests exist. The products used for this research are commonly and predominantly use products in our area of research and country. There is absolutely no conflict of interest between the authors and producers of the products because we do not intend to use these products as an avenue for any litigation but for the advancement of knowledge. Also, the research was not funded by the producing company rather it was funded by personal efforts of the authors.

REFERENCES

1. B.P. Bandga, S.A. Patil, B.L. Korbad, S.H. Nile, C.N. Khobragade, Eur. J. Med. Chem. 45,2629–2633 (2010) .
2. N.Sunduru, A. Agarwal, S.B. Katiyar, Nishi, N. Goyal, S. Gupta, P.M.S. Chauhan, Bioorg. Med. Chem. 14, 7706–7715 (2006).
3. Tatsuzaki, K.F. Bastow, K. Nakagawa-Goto, S.Nakamura, H. Itokawa, K.-H. Lee, J. Nat. Prod.69(10), 1445–1449 ,(2006) .
4. J.-M. Yun, M.-H. Kweon, H. Kwon, J.-K.Hwang, H. Mukhtar, Carcinogenesis 27(7), 1454–1464 (2006).
5. V. Calvino, M. Picallo, A.J. Lpoz- Peinado, R.M. Martin-Aranda, C.J.Duran-Valle, Appl. Surface Sci. 252(17), 6071–6074 (2006).

6. J.J. McKinnon, M.A. Spackman, A.S. Mitchell, Novel tools for visualizing and exploring intermolecular interactions in molecular crystals, ActaCryst. Section B 60 (2004) 627-668.
7. M.A. Spackman, D. Jayatilaka, Hirshfeld surface analysis, CrystEngComm 11 (2009)19-32.
8. M.A. Spackman, J.J. McKinnon, Fingerprinting Intermolecular Interactions in Molecular Crystals, CrystEngComm 4 (2002) 378-392.
9. K.S. Dhami and J.B. Stothers, Can. J. Chem., **1963, 43, 479**
10. K.S. Dhami and J.B. Stothers, Can. J. Chem., **1965,**43,510.
11. P.C Leuterbur, J .Am. Chem. Soc ., **1961,**83,1846.
12. Vincent Crasta, V. Ravindrachary, R.F. Bhajantri, Richard Gonsalves, J. Cryst. Growth 267 (2004) 129.
13. S. Gunasekaran, R. A. Balaji, S. Kumeresan, G. Anand and S. Srinivasan, Experimental and theoretical investigations of spectroscopic properties of N-acetyl-5-methoxytryptamine, Can. J. Anal. Sci. Spectrosc 53, 149 (2008).
14. S. S. Amiri, S. Makarem, H. Ahmar, and S. Ashenagar, Theoretical studies and spectroscopic
15. characterization of novel 4-methyl-5-((5-phenyl- 1, 3, 4-oxadiazol-2-yl) thio) benzene-1, 2-diol,J.Mol. Struct. 1119, 18 (2016).
16. M. Khalid, M. Ali, M. Aslam, S. H. Sumrra, M.U. Khan, N. Raza, N. Kumar, and M. Imran, Frontier molecular, Natural bond orbital, UV-Vis spectral study, Solvent influence on geometric parameters, Vibrational frequencies andsolvation energies of 8-Hydroxyquinoline, Int. J.Pharma. Sci. and Res., 8, 457 (2017).
17. G.R. Meredith, J. VanDusen, D.J. Williams, Optical and nonlinear optical characterization of molecularly doped thermotropic liquid crystalline polymers, Macromolecules 15 (1982) 1385–1389.
18. J.J. McKinnon, M.A. Spackman, A.S. Mitchell, Novel tools for visualizing and exploring intermolecular interactions in molecular crystals, ActaCryst. Section B 60 (2004) 627-668.
19. M.A. Spackman, D. Jayatilaka, Hirshfeld surface analysis, CrystEngComm 11 (2009)19-32.
20. M.A. Spackman, J.J. McKinnon, Fingerprinting Intermolecular Interactions in Molecular Crystals, CrystEngComm 4 (2002) 378-392.
21. L. Vivien, N. Izard, D. Riehl, F. Hache, E. Anglaret, Optical Limiting Properties of Suspensions of Single-Wall Carbon Nanotubes, AIP Conf Proc. 685 (2003) 559-563.
22. Brian S. Furniss, Antony J. Hannaford, Peter W.G. Smith and Austin R. Tatchell, Vogel's Textbook of Practical Organic Chemistry, Fifth Edition, Longman Scientific& Technical, UK, 1989.
23. J. C. Brice, The Growth of Crystals from Liquids, North-Holland Publishing Company, London, 1973.

24. J.P. Abraham, D. Sajan, V. Shettigar, S.M. Dharmaprakash, I. Nemec, I. Hubert Joe, V. S. Jayakumar, Efficient π-electron conjugated push-pull nonlinear optical chromophore 1-(4- methoxyphenyl)-3-(3,4-dimethoxyphenyl)-2-propen-1-one: A vibrational spectral study, Journal of Mol. Structure 917 (2009) 27-36.
25. Donald L. Pavia, Gary M. Lampman, George S. Kriz, Introduction to Spectroscopy, 3rd Edition, Thomson Learning, US, 2001.
26. P.S. Kalsi, Spectroscopy of Organic Compounds, 2nd Edition, Wiley Eastern Limited, New Delhi, 1995.
27. G.M. Sheldrick, ActaCryst. A short history of SHELX, A 64 (2008) 112-122.
28. C. Dong, PowderX: Windows-95-based program for powder X-ray diffraction data processing, J. Appl. Crystallogr. 32 (1999) 838-838.
29. M.A. Spackman, P. G. Byrom, A novel definition of a molecule in a crystal, Chem. Phys. Lett. 267 (1997) 215-220.
30. S.K. Wolff, D.J. Grimwood, J.J. McKinnon, M.J. Turner, D. Jayatilaka, M.A. Spackman, Crystal Explorer (Version 3.1), University of Western Australia, 2012.
31. J.J. McKinnon, D. Jayatilaka, M.A. Spackman, Towards quantitative analysis of intermolecular interactions with Hirshfeld surfaces, Chem. Commun. 37 (2007) 3814 – 3816.